Quasar Continuum Fitting and Silicon Absorption in the Low Redshift Intergalatic Medium

by

Adam A. Miller

Submitted to the Department of Physics
in partial fulfillment of the requirements for the degree of

Bachelor of Science

at the

MASSACHUSETTS INSTITUTE OF TECHNOLOGY

[June 2006]
May 2006

© Adam A. Miller, MMVI. All rights reserved.

The author hereby grants to MIT permission to reproduce and distribute publicly paper and electronic copies of this thesis document in whole or in part.

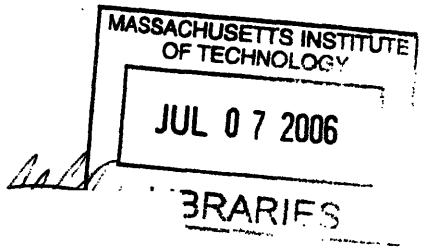

Author .....
Department of Physics
May 12, 2006

ARCHIVES

Certified by .....
Scott Burles
Assistant Professor
Thesis Supervisor

Accepted by .....
Professor David E. Pritchard
Senior Thesis Coordinator, Department of Physics

Quasar Continuum Fitting and Silicon Absorption in the Low Redshift Intergalatic Medium

by

Adam A. Miller

Submitted to the Department of Physics
on May 12, 2006, in partial fulfillment of the
requirements for the degree of
Bachelor of Science

Abstract

We present results on the evolution of Lyα absorption at low redshift, and the first systematic search for Si II absorption systems in the low redshift IGM. Our sample consists of 832 Lyα absorbers from 328 spectra of 204 QSOs taken from the *Hubble Space Telescope* archive. We develop a new, reproducible method of quasar continuum fitting, designed to quickly identify absorption lines and measure the relative line strength (a proxy for equivalent width). Our method, which fails to identify the weakest lines, does manage to detect the strong features in a given spectrum and provides enough information to identify metal absorption line systems. We confirm the results of previous studies of Lyα evolution at low redshift and find the number density of absorbers can be described by a power law in $(1+z)$ that is much flatter than that found for Lyα evolution at high redshift. Specifically, we measure a power law index of $\gamma = 0.57 \pm 0.16$ for lines with a rest relative line strength greater than 0.10 Å. We also identify the presence of 14 Si II systems at $z \sim 1$. The number of Si II 1193 and 1260 Å systems per unit redshift path length at a mean redshift of $z = 0.9$ is $< N(z) >= 1.6 \pm 0.6$. This density is similar to that found for C II, Mg II, and O VI absorbers.

Thesis Supervisor: Scott Burles
Title: Assistant Professor

Acknowledgments

I would like to thank Scott Burles for his comments, suggestions, and discussions about the content of this paper. And for putting up with me...

Contents

List of Figures

List of Tables

Chapter 1

Introduction

A particularly useful feature of quasi-stellar objects (QSOs) is that they provide a luminous background source to probe the intergalactic medium (IGM). Of particular interest is the Lyα forest where the majority of observable intergalactic H I gas resides. Investigating the distribution and evolution of hydrogen throughout the universe is vital towards understanding and creating models of galactic structure and formation. Several previous studies have characterized Lyα absorption at high redshift [1], [2], however, optical spectra are limited in the amount of information they can provide about low redshift Lyα absorption. From the ground, Lyα emission and absorption can only be observed at $z > \sim 2$. At lower redshifts Lyα becomes obscured by atmospheric interference. Therefore, to study Lyα absorption at $z < 2$ requires the ability to probe and the use of ultraviolet spectra.

Fortunately, the *Hubble Space Telescope* (*HST*) Faint Object Spectrograph (FOS), Goddard High Resolution Spectrograph (GHRS), and Space Telescope Imaging Spectrograph (STIS) are ideal for such studies of low redshift Lyα systems. Previously, a large survey identifying all H I and metal absorption lines has been conducted for all FOS QSO spectra [3], while the evolution of Lyα absorption lines at low redshift is also well studied [4], [5], [6], [7]. These projects are limited, however, in that they only include spectra from FOS. Each of these studies employs the use of hand fit continua to identify absorption lines in the IGM. While a well established method, hand fit continua are slightly problematic in that the method is not entirely reproducible.

Therefore, the possibility exists that two different people analyzing the same data in the same manner could still produce differing results. Hand fitting continua can also be a very laborious and time intensive practice. The development of a reproducible, computational method of continuum fitting would serve to unify the way in which Lyα absorption is measured, while at the same time drastically reducing the amount of time necessary to determine the continuum.

One particularly interesting difference between the ground-based and space-based observations of the Lyα forest is the dissimilarity in it's properties in the two different regimes. The distribution of Lyα absorbers in redshift, z, can be characterized by a power law in $(1+z)$. However, there seems to be a sharp break in the power law index at $z \sim 1.8$, with Lu, Wolfe, & Turnshek [1], and Bechtold [2] measuring a power law index of $\sim$1.7 for $z > 2$, while Weymann et al. [6], and Dobrzycki et al. [7] measure a power law index around 0.5 for $z < 1.7$. Characterizing the exact distribution of hydrogen over the history of the universe is vital to our understanding of cosmological evolution.

The presence of metal (anything that isn't H or He) absorption systems in the Lyα forest is well documented, however, there have been few direct searches for such systems. Formed in the cores of stars and later exploded into the surrounding IGM following the death of a star, metals can serve as possible tracers of supernovae by answering questions about when and where they occurred. A major problem in identifying metal gas clouds is that several of the stronger absorption lines are located in the Lyα forest where line blending and misidentification are significant difficulties in determining metal absorption line systems. Some of these issues are addressed by Burles & Tytler [8], in their search for O VI. Previous searches for Mg II [9], and C IV [4] have also been made. However, there have been no systematic searches for Si in the IGM, one of the most common elements in the universe after hydrogen and helium, despite several studies that have identified the presence of silicon [4], [5], [8], [6], and [3].

In this paper we expand upon the work of [7] to include all QSO observations taken with FOS, GHRS, and STIS. The goal is to generate the largest sample of low

redshift Lyα absorption lines to date. We develop a new, reproducible method for fitting the continuum of QSO spectra. In § 2 we present the data sample, along with the criteria for selection, and the reduction process. In § 3 we introduce our method of continuum fitting and line identification. We compare the method with hand-fit continua in § 4. Using the line list from § 3 we also measure and discuss the evolution of both Lyα and Si II at low redshift in § 4.

Chapter 2

Data

2.1 The Sample

Our sample consists of all known QSO spectra with $z > 0.33$ taken by *HST* FOS [10], GHRS [11], [12], and STIS [13]. We extend the sample of [14] to include all public data available from the *HST* STIS archive. The redshift limit was chosen such that the intrinsic Lyman limit (912 Å) is viewable by HST. Some QSOs were removed or omitted from our sample based on the following criteria:

1. Object is a known or suspected broad absorption line QSO.
2. Spectrum is high-resolution with small wavelength coverage (medium and high-res modes on both GHRS and STIS).
3. Low signal to noise (approximately ≤ 1 pixel^{-1}).
4. $z_{em} \geq 1.8$.[1]

Also, if two spectra in the sample provide almost identical wavelength coverage - for example, if both FOS G130H and GHRS G140L data are available - then only the higher quality spectrum is used. We include both spectra, however, in cases where there is only partial overlap - for instance, FOS G270H and FOS G160L.

[1]We elect to remove QSOs with a redshift greater than 1.8 because in this regime ground based optical observations provide better resolution and higher S/N of Lyα than *HST*.

After the selection criteria have been applied, our sample contains 328 different spectra of 204 QSOs.

2.2 Reduction

Before the continua were fit, each spectrum was processed by a series of steps described below:

1. The spectra were corrected for Galactic extinction.

2. Strong features not intrinsic to the QSO or absorption clouds are masked out, including instrumental artifacts, airglow, and cosmic rays.

3. The data are shifted into the QSO rest frame for continuum fitting.

Provided the correction for Galactic extinction comes before the data are shifted into the object's rest frame the order of the previous steps is unimportant. Below we discuss the steps in slightly more detail.

The Galactic extinction correction is based on the analytical form of [15] using $E(B-V)$ values from [16]. We assume that $R_V = 3.1$ for all QSOs.

The features that were not intrinsic to the QSO were masked by removing the individual pixels such that the code which performs the continuum fit ignores the bad pixels. If the masked pixels lied below the continuum following the fit then they were also masked from the search for absorption lines to prevent the false positive identification of non-lines.

Chapter 3

Continuum Fitting Technique

We introduce a new method of continuum fitting whereby the continuum at each pixel is determined by the weighted mean of the flux at that pixel and its nearest neighbors. The continuum is the convolution of the flux with a smoothing kernel, which is designed to be a half sine wave:

$$C_i = \sum_{j=0}^{m-1} F_{i+j-m/2}\ K_j \tag{3.1}$$

where C_i is the continuum at the i^{th} pixel, F is the flux, K is the smoothing kernel, and m is the total number of elements in the kernel. The kernel is normalized to unity and arranged such that the maximum amplitude of the half sine wave is always centered on the i^{th} pixel. At the edge of each spectrum the kernel is truncated such that only pixels which overlap the kernel are included in the sum. We employ the use of two smoothing kernels, which are identical in every feature except their width. The kernels were chosen to have a base width of 5000 km s^{-1} and 10,000 km s^{-1} at Lyα, or roughly 20 and 40 Å, respectively.

In Figures 3-1 and 3-2, we show 6 spectra and the fits produced by our method with the 5000 km s^{-1} smoothing kernel. We choose to only include the smaller of the two smoothing kernels to improve the clarity of the figures. The sample of QSOs shown is chosen to demonstrate the characteristics of the fits over a wide range in both QSO redshift and observed wavelength. We have also chosen 6 different *HST*

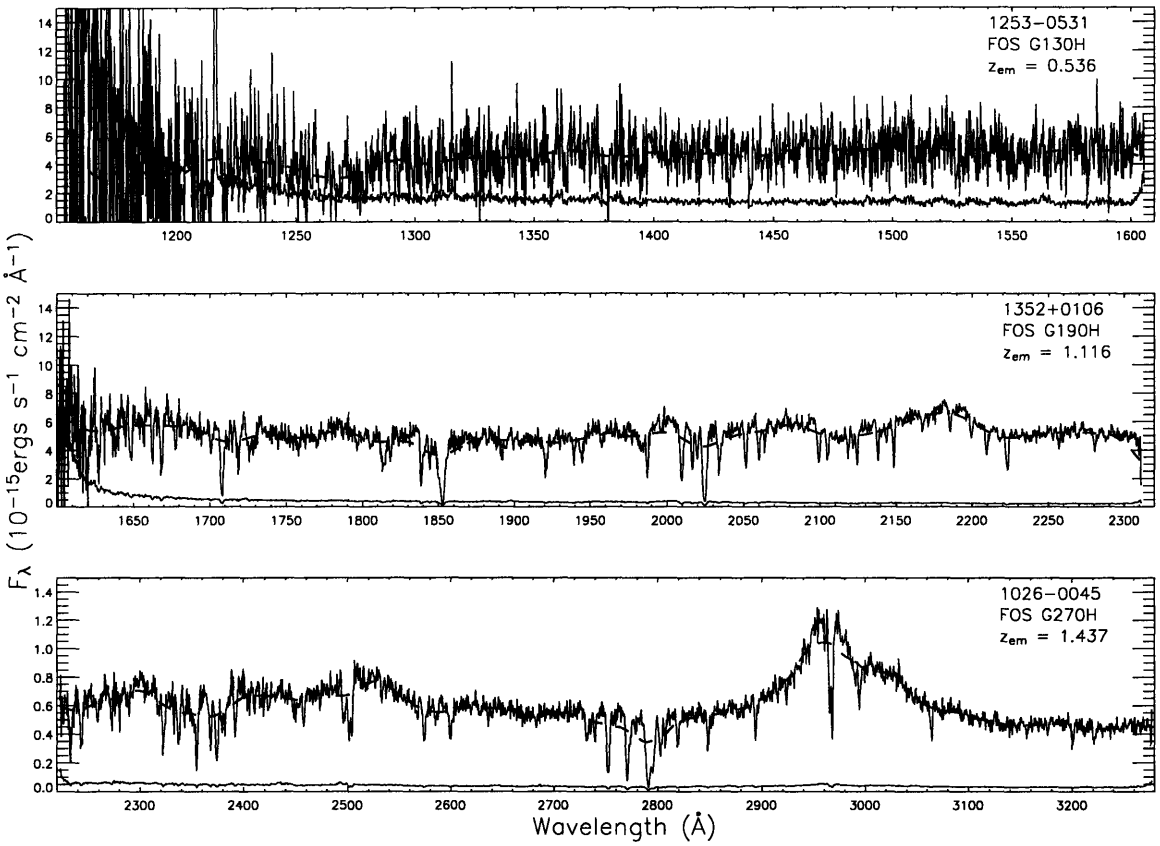

Figure 3-1: Spectra from 3 different QSOs plotted with the 5000 km s^{-1} kernel fitted continuum (dashed line) and 1 σ error.

gratings with a variety of intrinsic QSO features, especially Lyα and Lyβ emission.

We note that there are some limitations to this new method. While the smooth continuum will serve as a very good approximation of the "true" continuum in regions where there is no absorption or emission, the accuracy will suffer near strong features in the spectrum. By definition the continuum will always be underestimated near any absorption features (especially strong lines), because the reduced flux in these areas will pull the weighted mean down. For instance, see the strong features at $\sim$ 1215 Å in 2112+0555 and $\sim$ 2660 Å in 0126-0105 (Figure 3-2, and notice that the continuum is severely underestimated near these features. Conversely, in the vicinity of any strong emission features, which are intrinsic to all QSO spectra, our method will underestimate the true continuum at the peak of the feature and overestimate the true continuum on the edges, or wings, of the emission profile. This can be seen

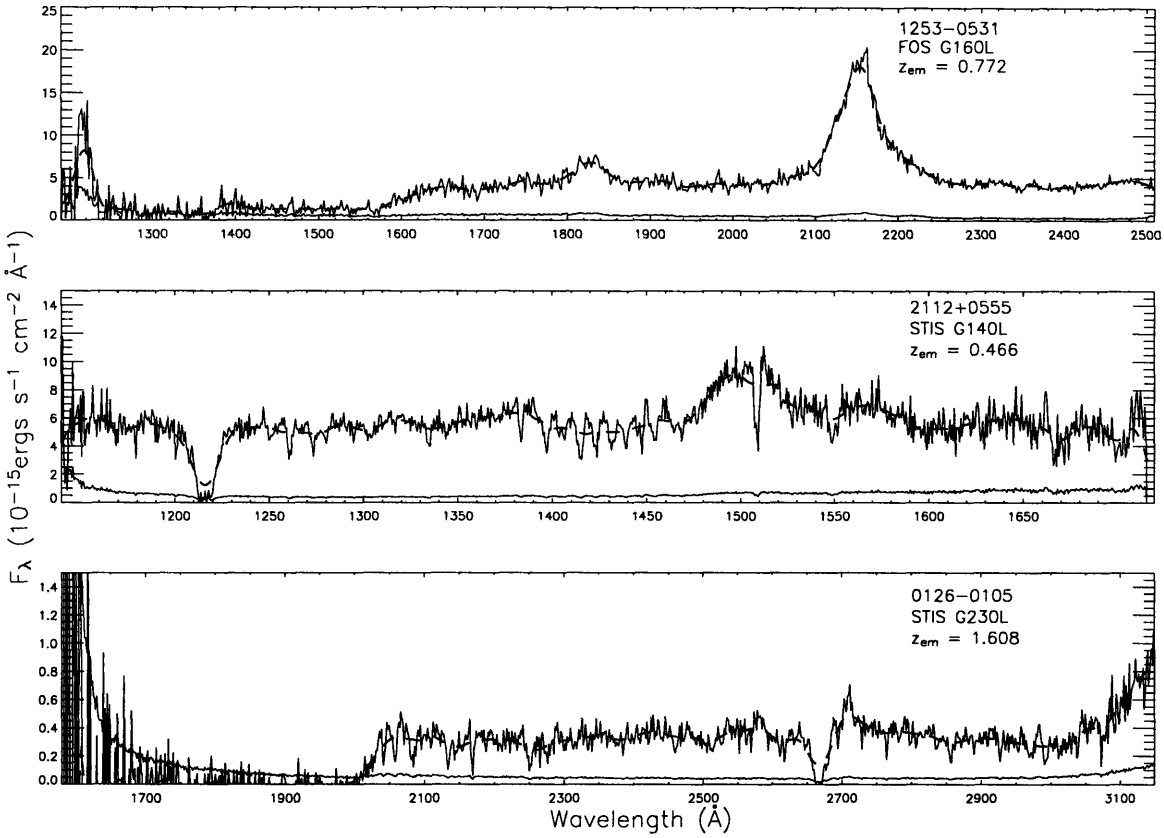

Figure 3-2: Spectra from 3 different QSOs plotted with the 5000 km s^{-1} kernel fitted continuum (dashed line) and 1 σ error.

near the Lyα and N v emission features ($\sim$ 2960 Å) in the spectrum of 1026-0045 (Figure 3-1).

It is possible to reduce these effects by changing the size of the kernel, however. A very wide smoothing kernel is less susceptible the effects of smaller absorption features, but at the same time it will do a terrible job of predicting the continuum near emission features. A narrow kernel would do a much better job fitting emission features, but it would also be extremely sensitive near absorption lines. It could potentially underestimate the continuum enough that real absorption lines no longer pass a significance test. In an effort to minimize the above effects we have elected to use two kernels of moderate width, as mentioned above. Despite the limitations mentioned above, our method is still employable for the identification of absorption lines, especially strong metal systems.

3.1 Line Identification and Equivalent Width Measurements

Using the method described above it would be impossible to accurately measure the equivalent width of any absorption lines in the spectra because our method does not replicate the "true" QSO continuum. Therefore we define a proxy for equivalent width - the relative line strength (RS), which is the relative absorption of a three pixel window at each pixel.

$$RS_i = \sum_{j=i-1}^{j=i+1} \frac{(C_j - F_j)}{C_j} \, \delta\lambda_j, \tag{3.2}$$

where RS_i is the relative line strength of the i^{th} pixel and $\delta\lambda_j$ is the width in Å of each pixel. We note that in the case of saturation the equivalent width will approach an upper limit equal to the size of the three pixel window. The uncertainty in RS_i is defined as the error in F_i for each pixel normalized to the value of the the continuum and added in quadrature. We define the significance level, SL, to be $RS/\sigma(RS)$, and consider any pixel with SL ≥ 3 to be a candidate for a line. We lastly require all pixels with SL ≥ 3 to be more significant than their two neighboring pixels on either side to qualify as an absorption line. The line centroids are measured by taking the weighted mean of the wavelength (Å) at the three pixels, where the weights are equal to the SL^2 at that pixel. While line centroids are typically determined using a gaussian fit to the absorption profile, this approach is not appropriate here because the continuum is underestimated. Thus, the assumption of gaussian absorption profiles is a bad one given that the continuum is underestimated at the wings of each absorption profile.

After applying these steps on every spectrum in our sample, we find that the two smoothing kernels measure approximately the same RS. Figure 3-3 shows the RS for the 10000 km s^{-1} filter vs. the RS for the 5000 km s^{-1} filter. Due to the difficulties of measuring the continuum near emission lines, as described above, we reject any lines near the two strongest emission features in QSO spectra: Lyα and C IV 1549 Å. Based on the average strength of each feature we reject any lines that fall in the range

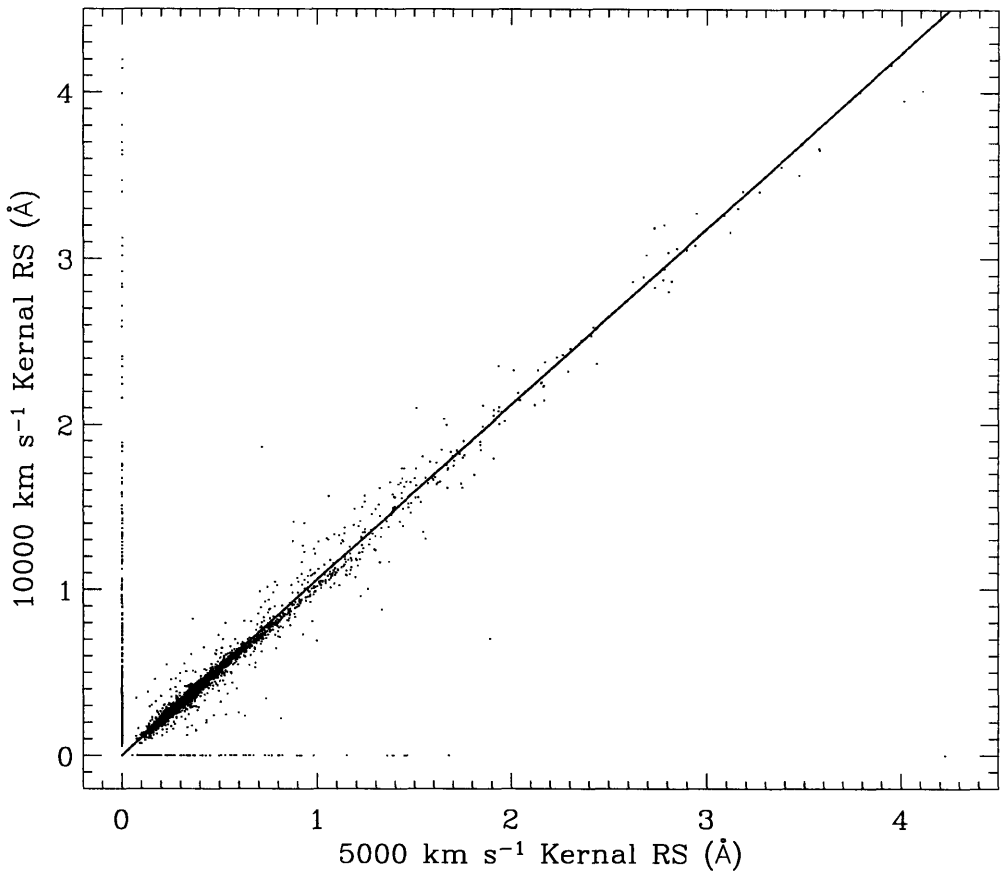

Figure 3-3: Scatter plot of RS as it is measured by both smoothing kernels. Points where $RS = 0$ indicate a line detected by only one kernel, as described in the text. The line represents the best fit to the points where $RS > 0$ for both kernels. It has a slope of 1.059.

1190 - 1250 Å or 1530 - 1570 Å in the rest frame of the QSO. We chose an asymmetric range about Lyα because N v 1240 Å, typically a strong feature when present, blends with the red side of Lyα and prevents a reliable measure of the continuum by our method until roughly $\lambda_{QSO} = 1250$ Å.

Following the above removal, we measure a total of 2157 absorption lines with both filters. The best fit line to these data yields a slope of 1.059 ($RS_{10000} = 1.059 \times RS_{5000}$), meaning the two methods measure roughly the same RS. The slightly higher RS for lines measured by the 10000 km s^{-1} kernel is to be expected given that this filter

averages over a larger range in λ and therefore will not be underestimated as much as the other filter at the location of the absorber. In addition to the 2157 lines measured by both filters there are 422 lines that were measured only by the 10000 km s^{-1} filter and 134 lines measured only by the 5000 km s^{-1} filter. These lines are shown in Figure 3-3 as having a reduced line strength of zero for the filter in which they were not detected. As can be seen from Figure 3-3 the majority of these are weak lines with 83.5% having a $RS < 1$ Å. Because the 5000 km s^{-1} filter is more selective, and therefore more likely to identify a higher percentage of real absorption features, we elect to use its line list for all further analysis in this paper.

Chapter 4

Results

4.1 Comparing the Smoothing Method with Hand Fit Continua

Measuring the continuum of a quasar with the method described in §3 is only useful if one has a sense of how the *RS* and the line lists are related to their analogous measurements made with the "true" continuum. Fortunately, Bechtold et al. [3] fit by hand the continua to all QSO spectra taken with FOS G130H, FOS G190H, and FOS G270H. Our sample and the sample of Bechtold et al. [3] have 159 spectra of 108 QSOs in common, this sample is large enough to compare our method with the hand fit method.

Figure 4.1 shows the observed *RS* vs. equivalent width as it was measured by Bechtold et al. [3]. The line represents the best fit to the data and has a slope of 0.378. Thus, assuming Bechtold et al. [3] fit the true continuum, an approximate conversion from *RS* to equivalent width can be made by multiplying the *RS* by the inverse of the slope, 2.646. There are a total of 2089 lines identified by both our method and Bechtold et al. [3]. In addition, there are 1678 lines measured by Bechtold et al. [3] alone. [1] Therefore, the smoothing method of §3 identified approximately 55% of those lines identified with the hand fit continua. Of the features only identified

[1] We note that [3] do not measure significance as $W/\sigma(W)$ and they include lines with a significance level < 3 in their lists. Only lines with SL > 3 are included in the line lists of this paper.

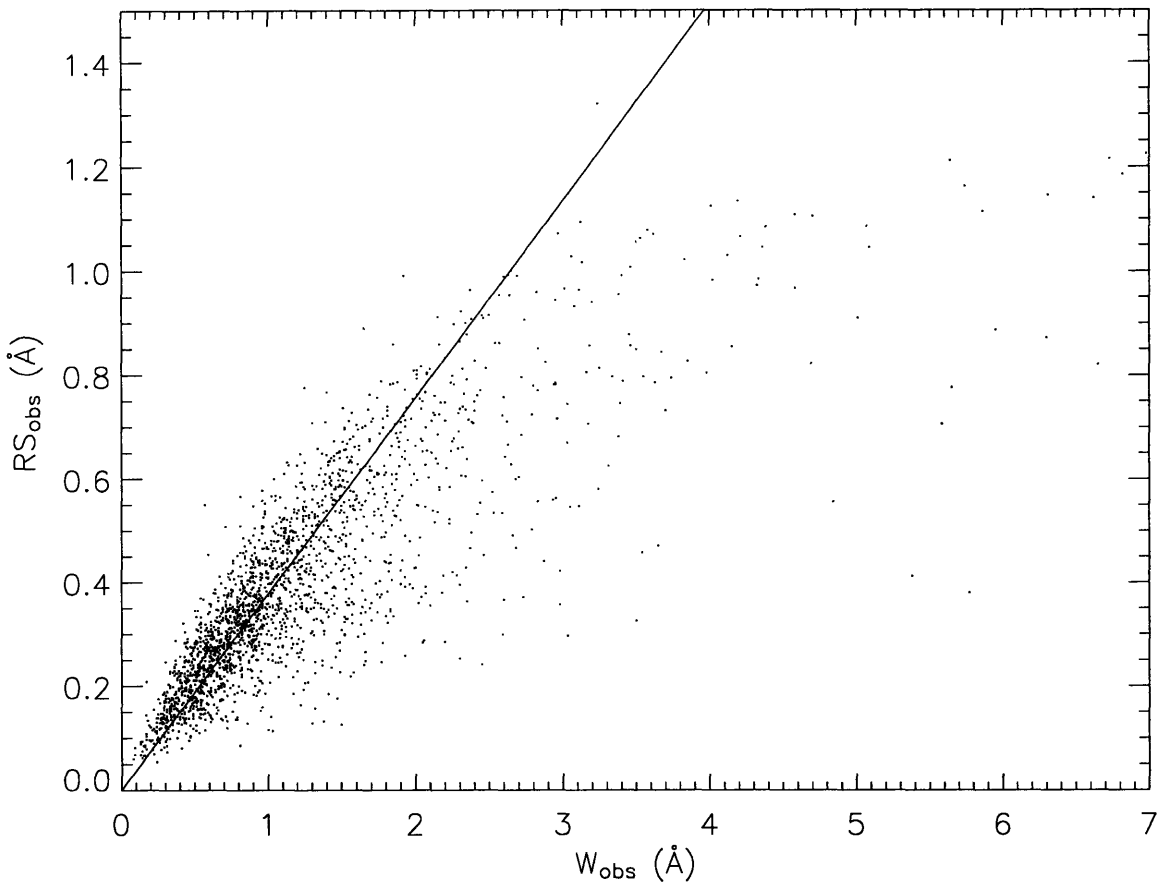

Figure 4-1: Scatter plot of the observed RS (this paper) vs. equivalent width (as measured by [3]). The line represents the best fit to the data.

by hand fit continua the majority are not strong features. For the lines that we did not detect the median W_{obs} is 0.47 Å and the median significance level is 5.5. Just over 85% of those lines detected solely by Bechtold et al. [3] have a significance level below 10. For comparison, Bechtold et al. [3] measures a median W_{obs} of 0.93 Å and a median significance level of 11.70 for the 2089 lines identified by both methods. Bechtold et al. [3] measures over 59% of the common lines at a significance level greater than 10. Clearly, the features we observed are stronger than those we missed.

We conclude that our method works well when searching for strong absorption features. While it is clear that we cannot perfectly resolve the equivalent width of an absorption feature using our method, it is possible to create a line list which is similar to that of the hand fit method. Also, given that virtually all the lines identified by

the smoothing technique are also identified by Bechtold et al. [3] (i.e. few artificial lines are measured by the method itself), our method provides a very quick way to search for Lyα absorbers with associated metal systems in the IGM.

4.2 Evolution of Lyα Absorbers at $z < 1.7$

We assume that the number of absorbers in the Lyα forest can be reasonably approximated by a power law in $(1+z)$. Specifically, we characterize the distribution of lines per unit redshift path length as:

$$\frac{dN}{dz} = A_0(1+z)^{\gamma} \tag{4.1}$$

where A_0 and γ are the distribution parameters. For a non-evolving population of clouds $1/2 \leq \gamma \leq 1$ [7]. Several previous ground based studies have established that $\gamma > 1$ for $z > \sim 1.7$. However, Weymann et al. [6] and Dobrzycki et al. [7] show that $\gamma < 1$ for $z < 1.7$.

Assuming a "ΛCDM" cosmological model for the universe, it is possible to calculate the value of γ as a function of redshift. Using Equation 13.42 from Peebles [17] we can characterize the number of absorbers per unit redshift for a non-evolving population as:

$$\frac{dN}{dz} = A_0 \frac{(1+z)^2}{E(z)} , \tag{4.2}$$

where

$$E(z) = \sqrt{\Omega_M(1+z)^3 + \Omega_\Lambda} , \tag{4.3}$$

and Ω_M is the mass density of the universe, and Ω_Λ is the dark energy density of the universe. If we set the right hand side of Equations 4.1 and 4.2 equal to each other, take the log of both sides and then differentiate with respect to $\log(1+z)$ we find:

$$\gamma(z) = 2 - \frac{3}{2}\frac{\Omega_M(1+z)^3}{\Omega_M(1+z)^3 + \Omega_\Lambda} . \tag{4.4}$$

Plugging in $\Omega_M = 0.27$ and $\Omega_\Lambda = 0.73$ [18] we find that $\gamma = 1.41$, 0.88, and 0.70 for

$z = 0.2$, 1.0, and 1.6, respectively. This suggests that over the range of redshifts we survey γ should be less than 1, in accordance with the work of [6] and [7].

Figure 4.2 shows the rest relative line strength, RS_{λ_0}, defined as $RS_{\lambda_0} = RS_{obs}/(1+z)$, of all Ly$\alpha$ lines as a function of redshift. The points marked with a cross are those that meet the specifications of the analysis carried out in § 4.2.1. The points indicate all the remaining SL ≥ 3 lines in the forest. We do not include any lines blue-ward of Lyβ emission ($\lambda_{QSO} = 1025.72$) to avoid confusion with potential Lyβ absorbers. We also remove any strong galactic absorption line features, including Si II λ1190, 1193, 1260, 1526, Si III λ1206, C II λ1334, C IV λ1548,1550, Al II λ1670, Fe II λ2344, 2374, 2382, 2586, 2600, Mg II λ2796, 2803, and Mg I λ2853.

Unfortunately, the uniformity of the sample across all redshifts is limited by the fact that all the observations were made by only a handful of telescope gratings. This leads to preferential treatment of QSO sight lines where the majority of the Lyα forest is located well inside the two edges of a grating. In addition to affecting the distribution of Lyα absorption redshifts, the path length, and minimum detectable equivalent width are also effected by the total number of sight lines associated with each grating [6]. In the appendix, Weymann et al. [6] provide a method to correct for the non-uniformity of the sample's coverage. They weight each component of the empirical cumulative distribution by the minimum 4.5 σ rest equivalent width at the location of the line. This correction cannot be applied here because it depends on the measurement of the "true" continuum, which is not what we described in § 3. Instead, we calculate the cumulative distribution function in terms of an "effective redshift path length" as described in [19], in which case every detected line increments the empirical distribution function by an equal amount.

4.2.1 The Cumulative Distribution as a Function of Redshift

We establish a minimum rest relative line strength of 0.10 Å for any lines that are to be included in our analysis of the distribution of Lyα absorbers. Using the conversion factor from above this RS threshold roughly corresponds to the 0.24 Å rest equivalent width threshold of [6] and [7]. We must also remove any lines where three times the

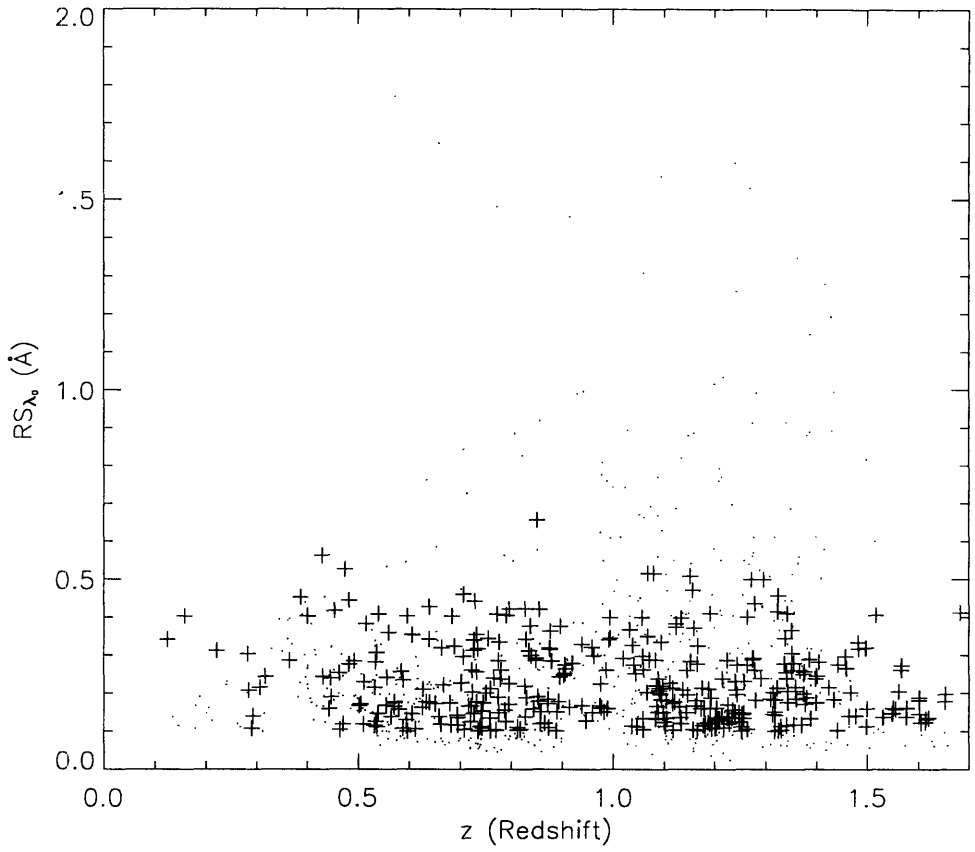

Figure 4-2: Rest relative line strength of all Lyα lines, forest and metal systems, vs. redshift. The crosses indicate the sample used to measure the empirical distribution function, as described in § 4.2.1, while the dots indicate the remaining 3 σ lines detected in the forest. Only points with a $RS < 2$ Å are shown.

signal to noise at that line is greater than the threshold minimum relative line strength to avoid over-counting the number of lines and the total path length. This results in the removal of many STIS lines where the S/N is high, but the three pixel window is relatively large, meaning we would be unable to detect a 3 σ line at the threshold RS of 0.10 Å. We also include all detected metal lines in our analysis. Since our line list is in all likelihood not complete, then our identification of metal systems would also be incomplete. To remove lines from an incomplete set of identifications could introduce a bias into the sample by removing only the strongest metal lines. Fortunately, Dobrzycki et al. [7] show that the inclusion of metal lines in the analysis of Lyα number density evolution has little effect on the results.

As can be seen from Figure 4.2.1, the power law fit to the data proves to be remarkably good. After applying a Kolmogorov-Smirnoff test to the data in Figure 4.2.1, we find there is a probability of 8% that a K-S statistic greater than or equal to the observed one would arise from a random sampling of true power law distributions of the same slope (or, $P_{KS} = 0.92$). The fit is performed by a computer algorithm that varies both γ and A_0 in order to maximize the K-S test statistic. The uncertainty in the fitting parameters is determined by assuming gaussian errors and measuring where the K-S test statistic has fallen to $e^{-1/2}$ of its maximum value.

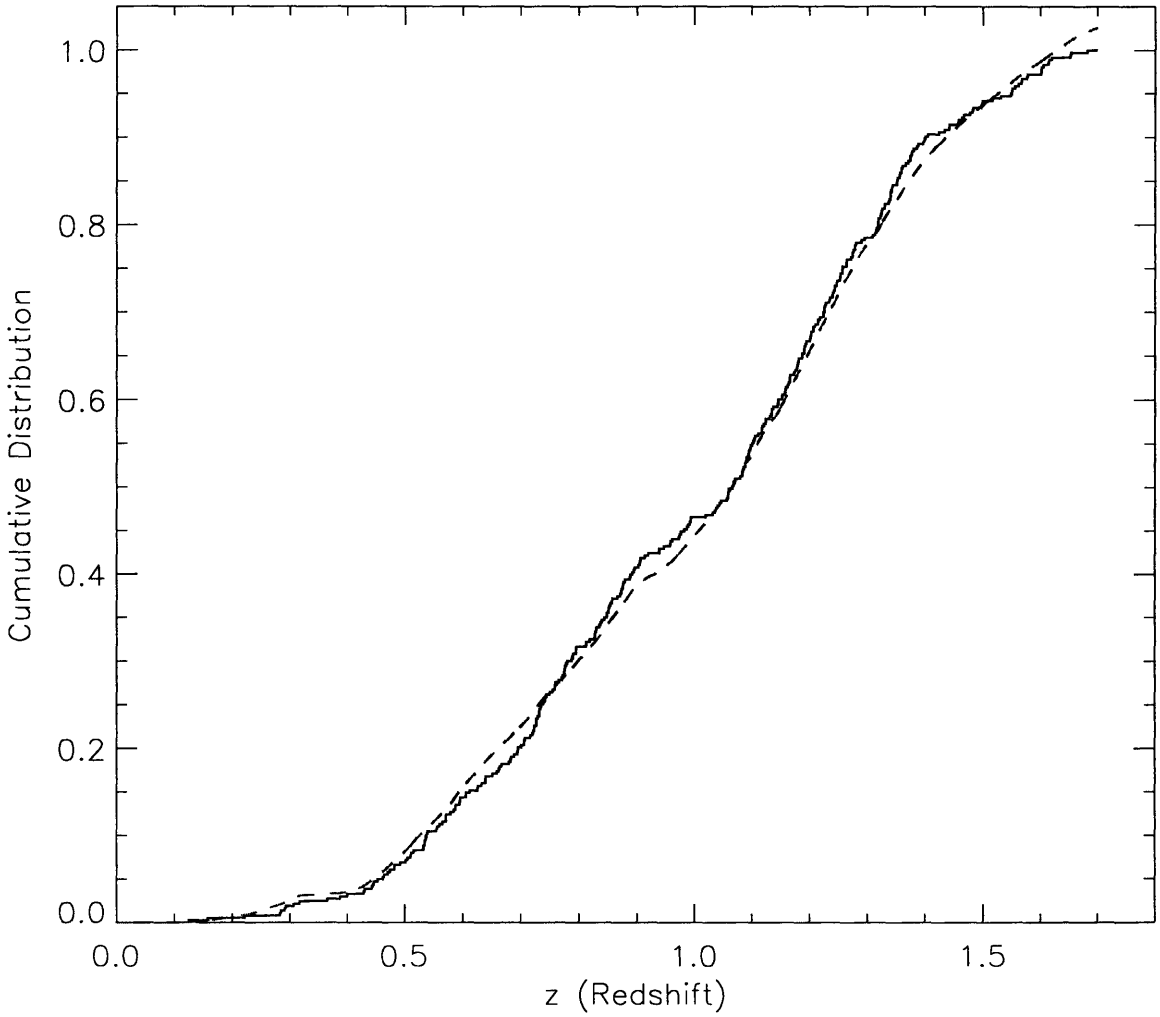

Figure 4-3: The cumulative distribution of Lyα forest lines, Lyα and metals lines, as a function of redshift. The solid line shows the cumulative distribution of absorbers, while the dashed line represents the best fit to the power law $17.3(1+z)^{0.56}$.

Our best fit to the data is consistent with the non-evolving case for Lyα absorbers at low redshift. Specifically, we find that $\gamma = 0.57 \pm 0.16$, with a corresponding value of A_0 equal to 17.3. These results are consistent with both [6] and [7], who find that γ is 0.26 ± 0.22 and 0.54 ± 0.21, respectively, for samples similar to our own. Dobrzycki et al. [7] explain how the difference in sample coverage leads to a slightly lower value of γ for [6]. These results are significantly lower than ground based studies of Lyα forest lines at a redshift greater than ~ 1.7. We also note that this disagrees with [20] who found that the break in dN/dz happens near $z \sim 1.2$. The largest discrepancy between our results and those of [6] and [7] is the value of A_0. We find that A_0 is significantly lower in our case than Dobrzycki et al. [7], who measures A_0 to be 32.7 for a sample similar to ours. We attribute this difference to largely different redshift coverage in the two samples. We elected to remove all QSOs with a redshift less than 0.33 which means we have very little coverage of the forest at extremely low redshifts. Weymann et al. [6] show that A_0 is extremely sensitive to the value of dN/dz near redshift 0; our limited coverage in this region is likely the cause of our relatively small value for A_0.

4.3 Si II Detection in the IGM

The search for low-ionized silicon in the IGM proves to be exceedingly difficult, because the strong lines Si II λ1190, 1193 and Si III λ1206 fall in the Lyα forest where the many Lyα lines and the high incidence of line blending can lead to many false positive identifications. Even the strong line at Si II λ1260 quickly becomes obscured by Lyα emission before entering the forest itself as the redshift of an absorbing system is decreased from the redshift of the QSO. Unless $z_{absorption} \sim z_{em}$ then Si II λ1260 suffers from the same problems as the other strong silicon lines.

To avoid the problems associated with misidentification and line blending we require that our test is tuned to minimize the number of missed Si II systems, while at the same time being very specific to minimize the number of false positives. We could severely limit the number of false positives by only considering the strongest lines.

Then we would miss many Si II lines, which would prevent us from predicting their overall frequency. False positives can be related to noise in the spectrum, or misidentified lines, especially Lyα. Therefore, we use three criteria for positive identification: line significance, redshift agreement, and the detection of at least three lines in the system.

4.3.1 Search for Si II Lines

The following procedure is used to search for Si II lines, identify possible redshift systems, and reject unreasonable ones:

1. We search for all systems with at least two 4.5 σ lines from the group Lyα, and Si II λ1193, 1260. We also require that all three lines from this group be detected at the 3 σ level. Lines are accepted into the system if they differ from the weighted mean z_{ave} by less than 0.001. The weighted mean z_{ave} is defined as:

$$z_{ave} = \frac{\sum_i w_i z_i}{\sum_i w_i}, \tag{4.5}$$

   where w_i is the weight placed on each line:

$$w_i = \frac{RS_{obs}^2}{\sigma(RS)^2}. \tag{4.6}$$

2. In systems with the three lines above we search for Lyβ, Si III 1206 Å, and C II 1334 Å in these systems. These are the most common lines associated with Si II systems from previous studies [3].

3. We require that Lyβ, Si III 1206 Å, and C II 1334 Å be 3 σ detections in order to be included in the system.

We elect not to include systems with only Si II lines, because the number of false identifications is similar to the the true number [8]. In fact, Burles & Tytler [8] show that the number of false systems in the Lyα forest dramatically decreases in the search for three-line systems instead of two-line systems, which is why we require the

presence of Lyα, and Si II λ1193, 1260. This is also what prevents us from searching for any lone Si III redshift systems. Despite the stringent criteria outlined above we note that there is no method which will throw out all false systems and keep all the real ones.

4.3.2 The Distribution of Si II

Table 4.1 shows the 14 systems in which we detected Si II, as well as the system at $z = 0.474$ in the sight line of QSO 0454-2203. This system has a well documented redshift system at $z = 0.474$ [3], and satisfies all the above criteria, with the exception of the fact that the Si II 1260 Å line falls within the region masked for Lyα emission. The same line is detected and identified as Si II 1260 Å by Bechtold et al. [3], however, so we include this system in the table for the reader's reference. This system is not included in any of the following analysis as it did not satisfy the necessary criteria for identification.

Table 4.1: Si II System Line List

Wavelength (Å)	ID (Å)	z_{obs}	RS_{obs} (Å)	$\sigma(RS)$ (Å)	SL[a]
0107-0232, $z_{em} = 0.728$, FOS G190H					
$z_{ave} = 0.55644$, $\sigma_z = 0.00688$					
1892.04.....	Lyα	0.55638	0.830	0.073	11.35
1857.25.....	Si II 1193	0.55641	0.307	0.072	4.25
1961.93.....	Si II 1260	0.55656	0.476	0.059	8.06
1878.05.....	Si III 1206	0.55661	0.507	0.069	7.33
2077.53.....	C II 1334	0.55674	0.554	0.021	25.90
0117+2118, $z_{em} = 1.493$, FOS G270H					
$z_{ave} = 1.16711$, $\sigma_z = 0.00336$					
2634.33.....	Lyα	1.16698	0.703	0.041	17.14

Continued on Next Page...

Table 4.1 – *Continued*

Wavelength (Å)	ID (Å)	z_{obs}	RS_{obs} (Å)	$\sigma(RS)$ (Å)	SL[a]
2586.23.....	Si II 1193	1.16731	0.352	0.057	6.19
2733.05.....	Si II 1260	1.16836	0.280	0.056	4.96
2224.33.....	Lyβ	1.16855	0.627	0.151	4.14
0454-2203, $z_{em} = 0.533$, FOS G190H					
$z_{ave} = 0.47436$, $\sigma_z = 0.00095$					
1792.34.....	Lyα	0.47436	0.776	0.024	32.48
1759.36.....	Si II 1193	0.47437	0.274	0.045	6.10
1857.99.....	Si II 1260	0.47410	...[b]	...[b]	...[b]
1512.10.....	Lyβ	0.47396	0.481	0.052	9.21
1778.70.....	Si III 1206	0.47426	0.370	0.039	9.45
1967.26.....	C II 1334	0.47412	0.429	0.025	17.21
0958+5509, $z_{em} = 1.750$, FOS G270H					
$z_{ave} = 1.10679$, $\sigma_z = 0.00120$					
2560.74.....	Lyα	1.10644	0.856	0.036	23.78
2514.65.....	Si II 1193	1.10732	0.465	0.069	6.74
2655.81.....	Si II 1260	1.10708	0.890	0.036	24.72
2541.30.....	Si III 1206	1.10634	0.799	0.041	19.73
1008+1319, $z_{em} = 1.287$, FOS G270H					
$z_{ave} = 0.90168$, $\sigma_z = 0.00196$					
2311.71.....	Lyα	0.90159	1.030	0.046	22.59
2270.16.....	Si II 1193	0.90244	0.376	0.081	4.64
2398.44.....	Si II 1260	0.90287	0.329	0.068	4.81
2539.30.....	C II 1334	0.90276	0.3121	0.064	4.85
1026-0045, $z_{em} = 1.437$, FOS G270H					
$z_{ave} = 1.29597$, $\sigma_z = 0.00138$					
2791.16.....	Lyα	1.29598	1.146	0.042	26.83

Continued on Next Page...

Table 4.1 – *Continued*

Wavelength (Å)	ID (Å)	z_{obs}	RS_{obs} (Å)	$\sigma(RS)$ (Å)	SL[a]
2739.68.....	Si II 1193	1.29590	0.325	0.074	4.42
2893.79.....	Si II 1260	1.29589	0.447	0.061	7.34
2354.36.....	Lyβ	1.29531	0.850	0.074	11.51
2770.74.....	Si III 1206	1.29651	0.993	0.047	21.07
3064.28.....	C II 1334	1.29614	0.434	0.063	6.87
1115+0802, $z_{em} = 1.718$, FOS G270H					
$z_{ave} = 1.04244$, $\sigma_z = 0.01052$					
2484.92.....	Lyα	1.04244	0.347	0.041	8.45
2436.64.....	Si II 1193	1.04195	0.257	0.053	4.81
2574.58.....	Si II 1260	1.04263	0.297	0.039	7.64
2462.94.....	Si III 1206	1.04139	0.591	0.039	15.31
2725.27.....	C II 1334	1.04213	0.161	0.039	4.17
$z_{ave} = 1.39440$, $\sigma_z = 0.00100$					
2911.21.....	Lyα	1.39474	0.162	0.039	4.19
2858.51.....	Si II 1193	1.39549	0.611	0.030	20.44
3017.31.....	Si II 1260	1.39389	0.827	0.028	30.07
2887.18.....	Si III 1206	1.39302	0.593	0.035	17.18
3196.41.....	C II 1334	1.39515	0.163	0.038	4.31
1229-0207, $z_{em} = 1.045$, FOS G190H					
$z_{ave} = 0.48967$, $\sigma_z = 0.01501$					
1811.64.....	Lyα	0.49024	0.518	0.078	6.68
1778.67.....	Si II 1193	0.49055	0.453	0.081	5.62
1875.86.....	Si II 1260	0.48828	0.452	0.073	6.18
1248+4007, $z_{em} = 1.030$, FOS G190H					
$z_{ave} = 0.73217$, $\sigma_z = 0.00465$					
2105.87.....	Lyα	0.73227	0.305	0.033	9.17

Continued on Next Page...

Table 4.1 – *Continued*

Wavelength (Å)	ID (Å)	z_{obs}	RS_{obs} (Å)	$\sigma(RS)$ (Å)	SL[a]
2067.14.....	Si II 1193	0.73230	0.177	0.039	4.59
2183.20.....	Si II 1260	0.73212	0.404	0.029	14.03
1775.82.....	Lyβ	0.73128	0.457	0.057	7.98
1352+0106, $z_{em} = 1.117$, FOS G190H					
$z_{ave} = 0.52395$, $\sigma_z = 0.00117$					
1852.61.....	Lyα	0.52394	0.855	0.029	29.16
1818.50.....	Si II 1193	0.52393	0.214	0.067	3.19
1921.02.....	Si II 1260	0.52411	0.399	0.051	7.89
1838.66.....	Si III 1206	0.52396	0.529	0.052	10.17
2033.86.....	C II 1334	0.52402	0.385	0.047	8.19
$z_{ave} = 0.66539$, $\sigma_z = 0.00103$					
2024.57.....	Lyα	0.66539	0.814	0.026	30.94
1987.32.....	Si II 1193	0.66540	0.469	0.042	11.01
2099.06.....	Si II 1260	0.66536	0.333	0.036	9.34
1708.32.....	Lyβ	0.66548	0.735	0.050	14.73
2009.54.....	Si III 1206	0.66559	0.541	0.037	14.62
2223.25.....	C II 1334	0.66594	0.397	0.030	13.19
1521+1009, $z_{em} = 1.321$, FOS G190H					
$z_{ave} = 0.67018$, $\sigma_z = 0.01672$					
2029.89.....	Lyα	0.66977	0.138	0.031	4.47
1993.39.....	Si II 1193	0.67049	0.232	0.033	7.12
2104.77.....	Si II 1260	0.66989	0.126	0.025	5.04
1538+4745, $z_{em} = 0.772$, FOS G190H					
$z_{ave} = 0.72931$, $\sigma_z = 0.00020$					
2102.27.....	Lyα	0.72931	0.764	0.012	65.60
2063.90.....	Si II 1193	0.72959	0.129	0.038	3.41

Continued on Next Page...

Table 4.1 – *Continued*

Wavelength (Å)	ID (Å)	z_{obs}	RS_{obs} (Å)	$\sigma(RS)$ (Å)	SL[a]
2179.59.....	Si II 1260	0.72925	0.204	0.017	12.14
1773.69.....	Lyβ	0.72921	0.652	0.035	18.41
2086.50.....	Si III 1206	0.72938	0.285	0.026	10.87
1630+3744, $z_{em} = 1.466$, FOS G190H					
$z_{ave} = 0.68712$, $\sigma_z = 0.01236$					
2050.32.....	Lyα	0.68658	0.283	0.041	6.98
2013.44.....	Si II 1193	0.68730	0.289	0.049	5.86
2126.94.....	Si II 1260	0.68748	0.265	0.036	7.39
2036.74.....	Si III 1206	0.68814	0.410	0.044	9.25

We evaluate the evolution of Si II systems in the IGM in a method similar to the one employed to measure the evolution of Lyα absorbers in § 4.2. We characterize the distribution of Si systems per unit redshift with a power law in (1+z). The sample of lines included in the search for Si II extends beyond the Lyα forest because some systems have Si II 1260 Å red-ward of Lyα emission, while others lie blue-ward of Lyβ emission. We restrict our search to all wavelengths greater than 1193 Å in the observed frame and less than 1260 Å in the QSO rest frame. For the cumulative redshift path length we require that spectral coverage for 1193 Å, Lyα, and 1260 Å in the rest frame of the absorber exist, and that three times the signal to noise is less than the threshold RS in each of the three corresponding pixels as well. We fit the number of absorbers to Equation 4.1 using the method of § 4.2.1.

[a]Significance level: $RS_{obs}/\sigma(RS)$

[b]We measure a 3 σ feature at the location of a Si II 1260 Å line in a $z = 0.47436$ cloud, however, this line falls in the region masked for the presence of Lyα emission. We include 0454-2203 in this table, because [3] identified a metal absorption system at $z = 0.474$ and because all other typical tracers of Si II (including Si II 1190 Å) are identified for this sight line. 0454-2203 is not included in the analysis of the number of Si II absorbers per unit redshift.

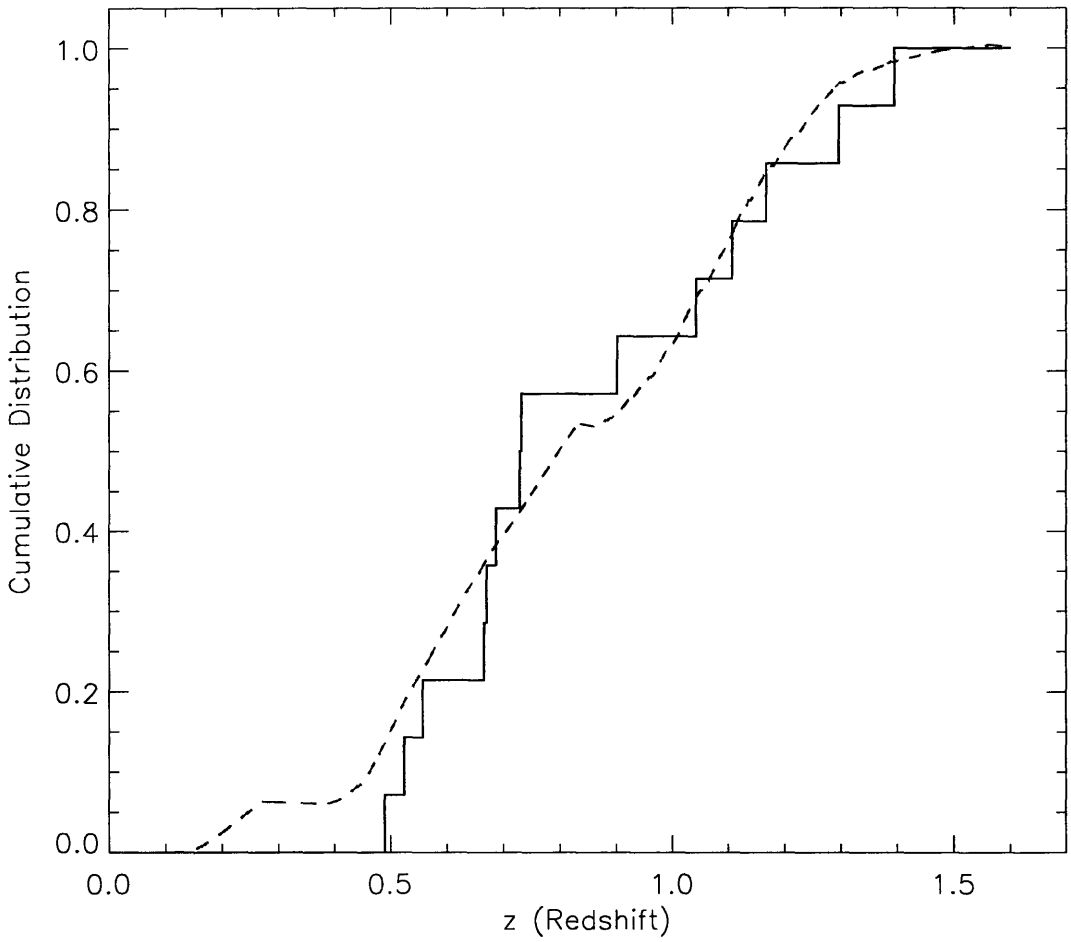

Figure 4-4: The cumulative distribution of Si II lines as a function of redshift. The solid line shows the cumulative distribution of absorbers, while the dashed line represents the best fit to the power law $2.1(1+z)^{-0.5}$. We note that there are large uncertainties in the fit due to the relatively small (14) number of total systems.

The cumulative distribution, as well as the best fit to a power law distribution are shown in Figure 4-4. We measure the fit parameters, and for the best fit case find $\gamma = -0.5 \pm 0.7$ and $A_0 = 2.1$. The K-S statistic for this fit is quite good, $P_{KS} = 0.92$. The uncertainty in γ is quite large, and this is believed to be the case because the sample size is quite small (only 14 identified systems). We note that in the case of Si II redshift systems a power law of the form of Equation 4.1 may not be the best way to parameterize the distribution of absorption systems per redshift. Our limited sample size does not allow us to conclude one way or another about the accuracy of the model.

We find the frequency of Si II in the IGM to be similar to the frequency of other commonly occurring metal systems in the IGM. We have identified 14 systems, and a total path length of $\Delta z_{total} = 10.72$. Evaluating these numbers at the mean redshift of all the systems ($z \sim 0.9$) we find the number density of Si II absorbers is

$$< N_{SiII}(z = 0.9) >= 1.6 \pm 0.6 \ . \tag{4.7}$$

Previous measurements of the number density of other common metal systems are also of order 1. Burles & Tytler[8] found that $< N(z = 0.9) >= 1.0 \pm 0.6$ for O VI, while Bachall et al. [4] found $< N(z = 0.3) >= 0.87 \pm 0.43$ for C IV, and Fan [9] found that $< N(z = 0.9) >= 1.0 \pm 0.25$ for Mg II. Our measurements show that the number density of Si II absorbers may be slightly higher than that of other common metal absorbers in the low redshift regime.

Chapter 5

Conclusion

We examined the absorption properties of the Lyα forest in the spectra of 204 QSOs. We identified 832 Lyα lines in these spectra, and found the evolution of hydrogen can be described by a power law in $(1+z)$ at low redshift. This power law is clearly flatter than those used to describe the evolution of Lyα at high redshift. This confirms the results of previous studies of low redshift Lyα evolution.

We also identified 14 Si II systems in the spectra of these QSOs. Si II absorption is as, if not more, common than O VI, C II, and Mg II at $z_{ave} = 0.9$. We measured the number density of Si II per unit redshift:

$$< N_{SiII}(z = 0.9) >= 1.6 \pm 0.6 \ . \tag{5.1}$$

Our search for both Lyα and Si II systems was conducted with a new continuum fitting method: we convolved the measured flux for a given sight line with a smoothing kernel designed to remove any sharp features (emission or absorption) from the spectrum. This method only provides an approximation to the "true" continuum, but we find that it is more than sufficient for identifying strong lines. Therefore, when searching for strong metal absorption systems in the spectra of QSOs our method is preferable to hand fit continua because it produces similar results in a much shorter amount of time. We note, however, that any precise measurements of equivalent width should be done using hand fit continua, or some other method beyond our

own.

Our method has some limitations, most notably near strong or sharp features in the measured spectrum, especially Lyα and C IV emission. Also, for sight lines with lots of absorption clouds, typically those with $z > 2$, which were not included in the analysis of this study, our method grossly underestimates the continuum and fails to identify what are clearly absorption features in the spectrum. It is also clear that the conversion from RS to equivalent width is invalid for these very strong lines. There are some cases where our method does a good job of approximating the continuum near emission features, however. For instance, when the rise of the feature is gradual and it has a relatively large width, our method, especially the 5000 km s^{-1} kernel, does a good job of approximating the continuum. We note that these cases are fairly few and far between.

We recommend that the method be used in the future for low or moderate absorption systems where the precise measurement of an absorption line's equivalent width is of secondary importance. Any time the measurement of the equivalent width is important, high resolution spectra should be used, rather than the low resolution spectra of this study. Further searches for Si II and other common intergalactic metals should be conducted to identify what percentage of Lyα absorbers are actually hydrogen, since the current typical assumption of 100% is not correct.

Bibliography

[1] Lu, L., Wolfe, A. M., & Turnshek, D. A. 1991, ApJ, 367, 19

[2] Bechtold, J. 1994, ApJS, 91, 1

[3] Bechtold, J., Dobrzycki, A., Wilden, B., Morita, M., Scott, J., Dobrzycka, D., Tran, K.-V., & Aldcroft, T. A. 2002, ApJS, 140, 143

[4] Bahcall, J. N., et al. 1993, ApJS, 87, 1

[5] Bahcall, J. N., et al. 1996, ApJ, 457, 19

[6] Weymann, R. J., et al. 1998, ApJ, 506, 1

[7] Dobrzycki, A., Bechtold, J., Scott, J., & Morita, M. 2002, ApJ, 571, 654

[8] Burles, S., & Tytler, D. 1996, ApJ, 460, 584

[9] Fan, X. M. 1995, Ph.D. thesis, Columbia Univ.

[10] Keyes, C. D. et al. 1995, "FOS Instrument Handbook", Version 6.0, (Baltimore: STScI)

[11] Ebbets, D. C., Brandt, J. C. et al. 1983, PASP, 95, 543

[12] Soderblom, D. R., et al. 1995, "GHRS Instrument Handbook", Version 6.0, (Baltimore: STScI)

[13] Kim Quijano, J., et al. 2003, "STIS Instrument Handbook", Version 7.0, (Baltimore: STScI)

[14] Telfer, R. C., Zheng, W., Kriss, G. A., & Davidsen, A. F. 2002, ApJ, 565, 773

[15] Cardelli, J. A., Clayton, G. C., & Mathis, J. S. 1988, ApJ, 329, L33

[16] Schlegel, D. J., Finkbeiner, D. P., & Davis, M. 1998, ApJ, 500, 525

[17] Peebles, P. J. E. 1993, Principles of Physical Cosmology (Princeton, NJ: Princeton University Press), 323

[18] Spergel, D. N. et al. 2003, ApJS, 148, 175

[19] Storrie-Lombardi, L. J., McMahon, R. G., Irwin, M. J., & Hazard, C. 1996, ApJ, 468,121

[20] Kim, T.-S., Cristiani, S., & D'Odorico, S. 2001, A&A, 373, 757